Journal of Electronic Materials (2022) 51:1922–1932
https://doi.org/10.1007/s11664-022-09535-5

TOPICAL COLLECTION: SYNTHESIS AND ADVANCED CHARACTERIZATION OF MAGNETIC OXIDES

Electronic Structure, Photoluminescence and Thermoluminescence Studies of Cu-Doped $Mg_2B_2O_5$ Nanophosphors

Jitender Kumar[1] · Aditya Sharma[2] · Sung Ok Won[3] · Keun Hwa Chae[3] · Chander Shekhar[1] · Shalendra Kumar[4,5] · Ankush Vij[4]

Received: 5 December 2021 / Accepted: 17 February 2022 / Published online: 15 March 2022

Abstract

We synthesized Cu-doped $Mg_2B_2O_5$ nanophosphors using a combustion method, and investigated their structural, morphological, optical band gap, electronic structure, and photo/thermo-luminescence properties using x-ray diffraction (XRD), selected area electron diffraction (SAED), high-resolution transmission electron microscopy (HR-TEM), diffuse reflectance spectroscopy (DRS), x-ray absorption near-edge structure (XANES) spectroscopy, photoluminescence (PL) spectroscopy, and thermoluminescence (TL) glow curves. Rietveld refinements of the XRD patterns confirmed the formation of single triclinic phase (space group P-1) for the pure and doped $Mg_2B_2O_5$ nanophosphors. Variations in the cell parameters as a function of dopant concentrations has been determined. The HR-TEM images confirmed the formation of aggregated particles of unusual morphology. The SAED pattern also confirmed the triclinic phase in Cu-doped $Mg_2B_2O_5$ nanophosphors. The band gap of the Cu-doped samples decreased from 5.18 eV to 5.10 eV. The XANES study at the Cu L-edge confirmed the Cu^{2+} ions in the Cu-doped $Mg_2B_2O_5$ nanophosphors. The O K-edge spectrum of pure $Mg_2B_2O_5$ confirmed the existence of marginal oxygen vacancies in the sample, which increases after Cu incorporation in the $Mg_2B_2O_5$ nanophosphors. Peak position variation in the O K-edge confirmed the modified hybridization among the O 1*s* to O 2*p* transitions. From the PL studies and CIE chromaticity diagram, a yellow-reddish color emission from the Cu-doped $Mg_2B_2O_5$ was observed. The TL glow curves obtained after gamma irradiation of the samples were used to evaluate the order of kinetics, activation energy, and frequency factor. The present results infer that Cu-doped magnesium pyroborate could be a potential candidate for solid-state lighting and radiation dosimetry-based applications.

✉ Shalendra Kumar
shailuphy@gmail.com

✉ Ankush Vij
vij_anx@yahoo.com

[1] Nanophosphors Lab, Department of Physics, Amity University Haryana, Gurgaon 122413, India

[2] Department of Physics, Manav Rachna University, Faridabad, Haryana 124001, India

[3] Advance Analysis Centre, Korea Institute of Science and Technology (KIST), Seoul 02792, South Korea

[4] Department of Physics, University of Petroleum and Energy Studies, Dehradun, Uttarakhand 248007, India

[5] Department of Physics, College of Science, King Faisal University, Hofuf, Al-Ahsa 31982, Saudi Arabia

Graphical Abstract

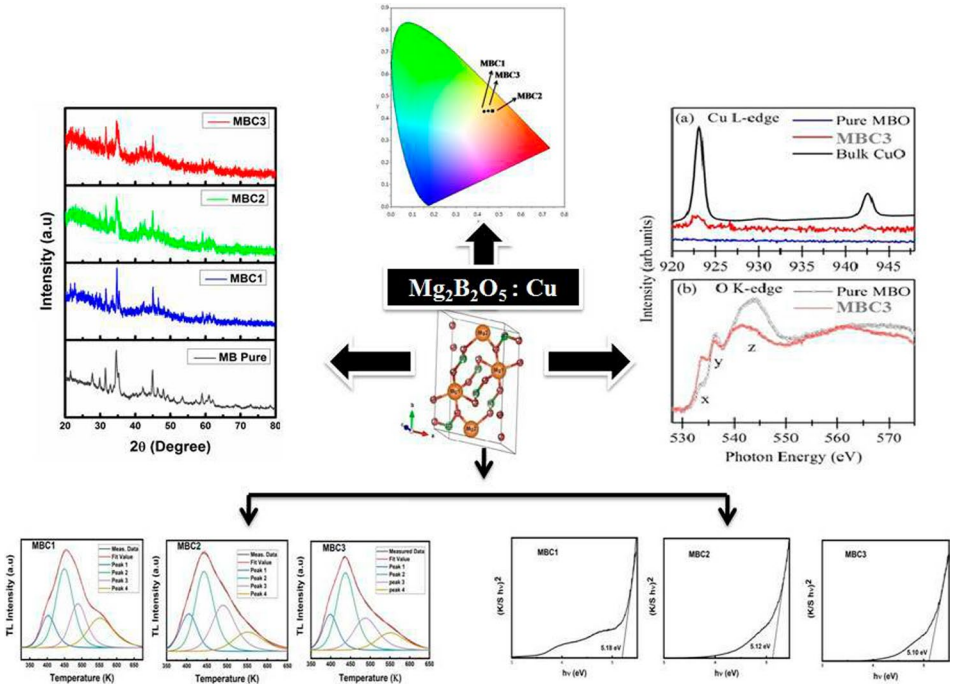

Keywords $Mg_2B_2O_5$ nanophosphors · XANES · thermoluminescence · photoluminescence · diffuse reflectance spectroscopy

Introduction

Borates are of great interest with their long involvement in the areas of metal, ceramics, refinement of gold and silver, adhesives, pharmaceuticals, abrasives, cosmetics, anticorrosion compounds, and insecticides.[1] Borate compounds have been used in applications across various fields of high technology, like nonlinear optics, mechanical strength, laser technology, and plasma display due to the stability of borate-based compounds in different phases and crystal structure with tunable crystallinity.[2,3] Of all the borates, metal borates are especially of great interest due to their unique properties, like chemical inertness, high mechanical strength and high Young's modulus, low thermal expansion coefficient, super insulation, light weight, and high corrosion resistance.[4–10] Among metal borates, magnesium borate compounds have gained the attention of the scientific community as they have excellent mechanical and thermal stability. Magnesium borate forms various compounds, for example, $Mg_2B_2O_5$ (nanowire, nanorod, and whisker 1-D nanostructures), MgB_4O_7 (nanowire), and $Mg_3B_2O_6$ (nanotube). Different properties of these compounds have been used as wide band gap semiconductors, antiwear additives, and electronics ceramics.[11–15] MgB_4O_7 both pure and doped with dysprosium have been used in medical dosimetry due to the low effective atomic number, as well as having about 2.2 times higher sensitivity compared to TLD-100.[16,17] Magnesium pyroborate ($Mg_2B_2O_5$) nanostructures have been used in wear-resistant materials, wide band gap semiconductors, in anticorrosion, as scintillators, discharge lamps, and reducing friction additives due to their inhibiting properties, like being flame-retardant, having high thermal and mechanical strength as highly conductive multi-functional solid state electrolytes, and having good microwave dielectric properties.[18–24] Zeng et al. studied $Mg_2B_2O_5$ for lubricating properties and concluded that the material could be used as a promising antiwear additive.[25] Qasrawi et al. determined the band gap of $Mg_2B_2O_5$ synthesized using a partial precipitation method to be 4.72 eV.[26] Awatif et al.[27] prepared europium-doped $Mg_2B_2O_5$ by mixing stoichiometric amounts of europium oxide and $Mg_2B_2O_5$ nanowires by a solid-state reaction method at 930ºC in air. Eu-doped $Mg_2B_2O_5$ has been used as a UV emitter and green phosphor.[27] Recently, Kumar et al.[28–30] studied the photoluminescence and thermoluminescence properties of pure and Eu-doped magnesium pyroborate irradiated with gamma radiations and UV radiations (λ = 365 nm and 254 nm), and correlated with electronic structures probed using x-ray absorption near-edge

spectroscopy studies. X-ray absorption spectroscopy has confirmed the oxidation state of dopants introduced in host materials. Researchers have earlier studied pyroborate containing magnesium through magnetization and electroparamagnetic measurements, which showed promising results.[31,32] Copper is among the promising dopants that enables the creation of defects leading to enhanced thermoluminescence of the host material, as it acts as a luminescence center.[33,34] Although there are a few studies on magnesium pyroborate as mentioned above, it has yet to be investigated in detail as magnesium tetraborate for luminescence applications using various dopants.

In the present paper, Cu-doped $Mg_2B_2O_5$ nanophosphors have been prepared using combustion synthesis. The prepared samples were characterized by x-ray diffraction (XRD), transmission electron microscopy (TEM), selected area electron diffraction (SAED), and high-resolution transmission electron microscopy (HR-TEM) for structural characterization and phase analysis along with Rietveld refinement of the obtained XRD patterns. Diffuse reflectance spectroscopy (DRS) was performed to determine the band gap of Cu-doped magnesium pyroborate as a function of dopant concentration. Thermoluminescence (TL) glow curves of the prepared samples irradiated with gamma radiation at different doses were investigated to obtain the kinetic parameters. Photoluminescence (PL) spectroscopy analysis was carried out at a 325-nm excitation wavelength, and the response of emission spectra was studied.

Experimental

Combustion synthesis technique was used for synthesis of Cu-doped $Mg_2B_2O_5$ nanophosphors at various concentrations of dopant. Synthesis of Eu-doped $Mg_2B_2O_5$ nanophosphors using a combustion technique has already been reported elsewhere.[28] In this technique of the synthesis of nanophosphors, exothermic reaction leads to the formation of the desired product in the presence of some fuel, which fits best for reactions like urea, glycine, etc. This process has advantages over other processes as it is less time-consuming and occurs at relatively low temperature. In the present work, magnesium nitrate hexahydrate, copper nitrate tri-hydrate, and lithium nitrate were mixed with boric acid, ammonium nitrate, and urea (fuel) as per the stoichiometric ratio corresponding to 0.1% Cu, 0.2% Cu, and 0.3% Cu in the $Mg_2B_2O_5$, and the samples have been labeled MBC1, MBC2, and MBC3, respectively. The reagents were mixed and properly ground in an agate mortar and pestle to form a homogeneous mixture. The appropriate amount of the homogeneous mixture was taken in a china dish and kept in a muffle furnace preheated at 200ºC. The furnace was then heated up to 600ºC at which the combustion reaction starts, leading to the decomposition of the nitrates and subsequent release of fumes and flames from the sample mixture. Upon completion of the combustion, the hot and dry remains along with the china dish were kept on a metal plate for quenching. The powder obtained in this process was again ground and then annealed at 400ºC in air. The samples thus obtained were again ground and put in dry small tubes. Synthesis of pure $Mg_2B_2O_5$ nanophosphors using a combustion technique has already been reported elsewhere.[35]

Characterization

A D-8 Advance Bruker diffractometer generating Cu-Kα radiations with an energy of 8.04 KeV and a wavelength of 1.5406 Å was used to record the XRD patterns. TEM images were recorded on a JEOL JEM-F200 (200KV cold FEG-based TEM; IUAC, New Delhi, India). DRS of all the synthesized samples was performed on a set up in the range of 200–700 nmon (RIMS; RIII, India) . Soft x-ray absorption near-edge structure (XANES) spectra at the Cu L-edge and O K-edge were collected using a 10D XAS-KIST soft x-ray beamline (Pohang Accelerator Laboratory, South Korea. The surface sensitive mode of data collection, i.e., total electron yield mode, was applied for collecting the XANES data. The resolution of beam line, detailed procedure of data collection, background removal, data normalization, and other technical details of the beam-line operation are provided elsewhere.[36]

For the TL, all the samples were exposed to different dosages of gamma radiation using a Co^{60} source. Before gamma exposure, the samples were annealed at 400ºC for 30 min to remove any residual information, which might be due to moisture or due to exposure to light. After the desired exposure, TL glow curves were recorded on a Harshaw Model 3500 TLD Reader having a neutral density filter, taking 5 mg of the sample each time in a nitrogen atmosphere at a heating rate of 5 K/s at the Health Physics Laboratory, IUAC, New Delhi, India). PL spectra were recorded using a Renishaw in-Via Raman microscope at an excitation of 325 nm line of the He-Cd laser.

Results and Discussion

Structural Analysis

XRD patterns of the samples were obtained to analysis structural information including crystallite size and phase formation. The XRD patterns confirmed the formation of single-phase in triclinic crystal structures matching with the JCPDS card no 150537. Crystallite sizes obtained from Debye Scherer's formula were found to be 19 nm (MBC1),

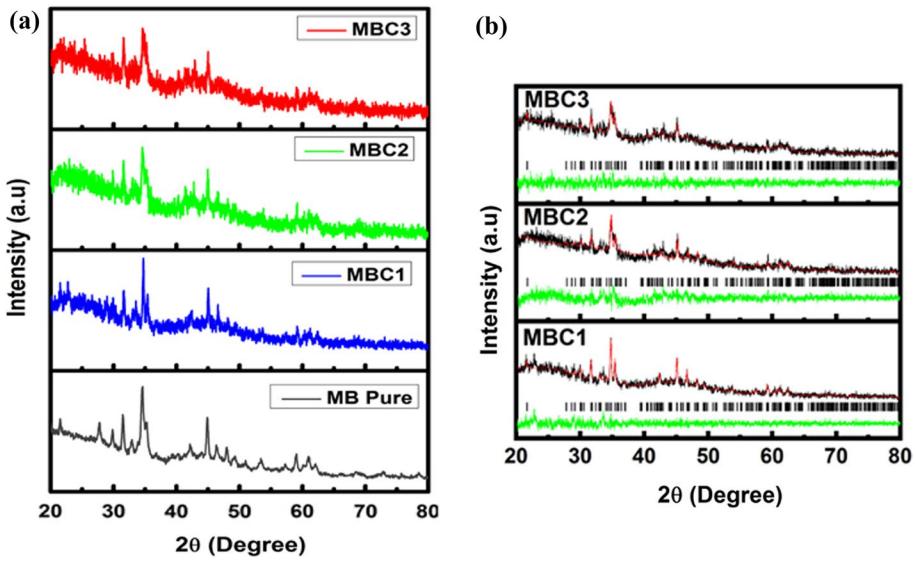

Fig. 1 (a) XRD patterns of pure and Cu (0.1, 0.2, and 0.3%)-doped $Mg_2B_2O_5$ nanophosphors. (b) Rietveld refinement of Cu-doped $Mg_2B_2O_5$ nanophosphors.

Table I Information retrieved from the Rietveld refinement of Cu-doped magnesium pyroborate nanophosphors

Sample	A	b	c	A	B	Γ	Cell volume	Chi^2	R_p	R_{wp}	R_e
MBC1 (Gof-1.1)	6.1548	9.2172	3.1204	90.473	92.188	104.457	171.2730	1.14	9.07	11.6	10.9
MBC2 (Gof-1.1)	6.1396	9.1947	3.1149	90.590	91.785	104.479	170.1479	1.34	10.2	12.9	11.2
MBC3 (Gof-1.1)	6.1515	9.2098	3.1204	90.375	92.251	104.324	171.1317	1.18	9.16	11.8	10.9

24 nm (MBC2), and 32 nm (MBC3) for different Cu-doped (0.1–0.3%) magnesium pyroborate nanophosphors. The grain size has been found to increase proportionally with the Cu-dopant concentration. The phases of the samples remain unaltered with the change of the concentration of the dopant, implying that the concentration is well within the solubility limit for the dopants.

Rietveld refinement of the synthesized samples doped with copper is shown in Fig. 1b. Information retrieved from the Rietveld refinement shows the presence of magnesium and oxygen vacancies in $Mg_2B_2O_5$: Cu (0.1–0.3%). Here, also, non-linear variation of volume and cell parameters has been observed with the change in concentration of the dopants. Convergence indicators, e.g., chi^2 and goodness of fit along with cell parameters and cell volume are listed in Table I, which shows variations of the unit cell volume with the concentration of the dopant. The cell volume initially increases and then decreases, and, on further increment in the concentration of the dopant, again increases, but this increment and the decrement in later ones are quite small so that they seem nearly constant throughout. This indicates that, on the addition of Cu to the lattice, Mg atoms are replaced by Cu and the concentration of Cu atoms decreases on further increments due to concentration-quenching. $A_2B_2O_5$ (A = Mg,Co) has apparently a one-dimensional structure in which A is surrounded by 6 oxygen atoms and

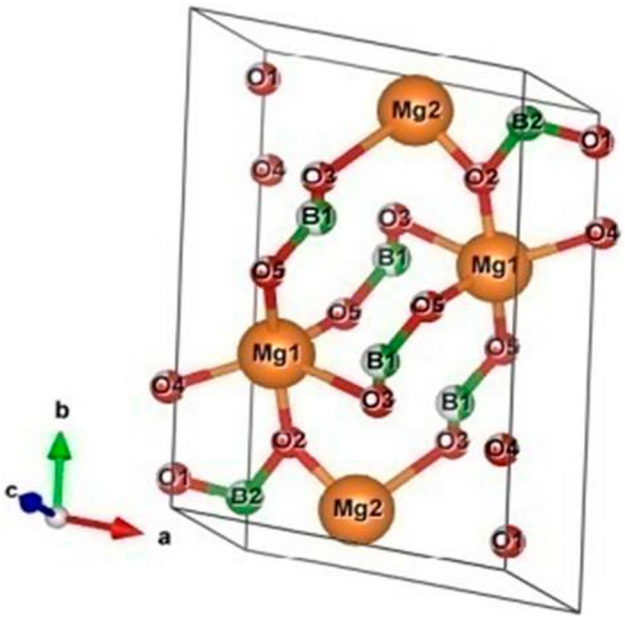

Fig. 2 Crystal structure of $Mg_2B_2O_5$: Cu (0.3%).

B is surrounded by 3 oxygen atoms, as shown in Fig. 2 for MBC3.[37,38] Table II shows normalized vacancies at the lattice positions for the samples gathered from the Rietveld refinement.

Microscopic Analysis

In order to get insights into the morphology and particle size of the Cu-doped samples, TEM analysis has been carried out on the MBC3 sample. TEM images show the formation of elongated, non uniform, asymmetric, and agglomerated nanocrystals with a size range between 55 nm and 126 nm and average particle size as 80 nm, as shown in Fig. 3.

Table II Normalized vacancies of atoms obtained after Rietveld refinement

Atom	Normalized occupancy		
	MBC1	MBC2	MBC3
O1	0.811237	0.787343	1
Mg2	0.782424	0.164774	0.659165
B2	1	0.498675	0.764025
B1	0.434054	0.579512	0.478067
O5	0.734197	0.825285	0.795264
Mg1	0.723998	1	0.988627
O3	0.505086	0.571071	0.683064
O4	0.653001	0.826996	0.843452
O2	0.666863	0.863871	0.856359

The HR-TEM images were analyzed using Image-J software, and the calculated d spacing was found to correspond to the lattice plane (110) of triclinic $Mg_2B_2O_5$ nanophosphors. SAED was also carried out, and the calculated d spacing was found to correspond to $(\bar{1}\,20)$ of triclinic $Mg_2B_2O_5$. Both HR-TEM and SAED images clearly show the formation of a single phase triclinic structure of MBC3.

Diffuse Reflectance Spectroscopy

DRS images for all the prepared samples are shown in Fig. 4. The band edge absorption was observed around 250 nm, which corresponds to the band gap of magnesium pyroborate. In the DRS of MBC1, broad absorption has been observed in the range of 300–350 nm, which may be due to magnesium and oxygen vacancies, as discussed in Structural Analysis Section.

As concentration of dopant is increased, defect- or vacancy-assisted broad absorption around 300-350 nm decrease continuously as the addition of Cu acts as a donor and suppresses the formation of defect states.

To determine the band gap of samples synthesized in the present study, first the reflectance is converted into absorption using the Kubelka–Munk equation:

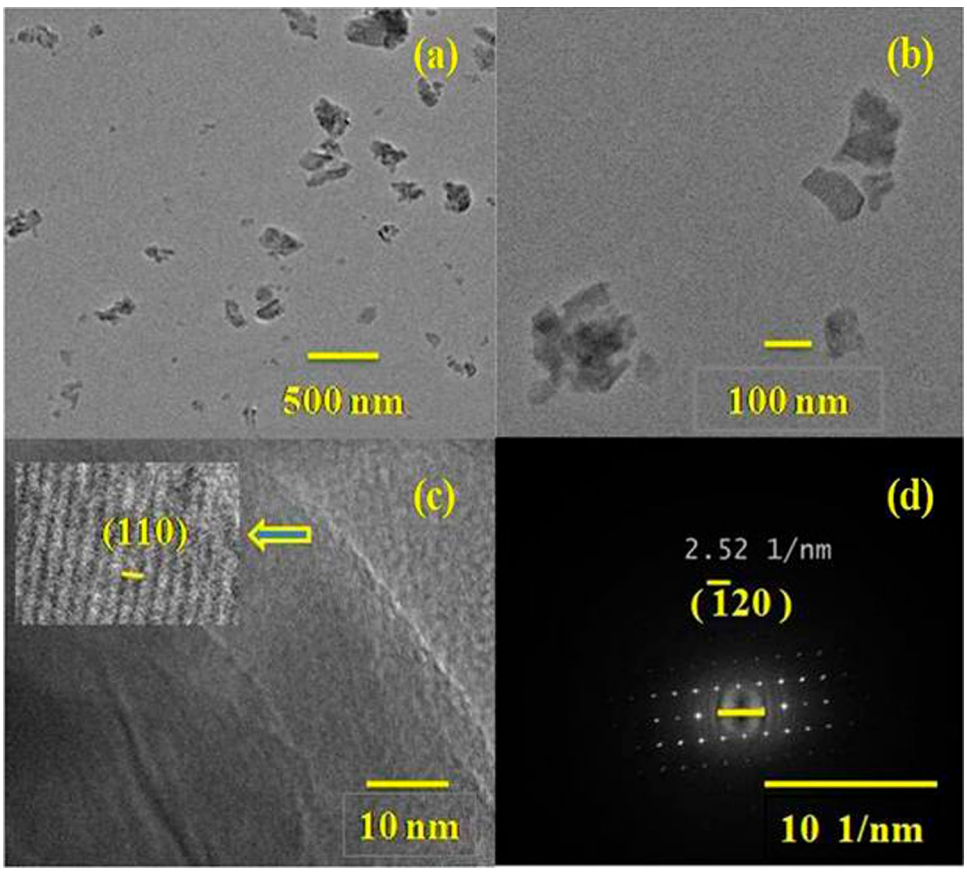

Fig. 3 (a) TEM image, (b) magnified TEM image, (c) HR-TEM image, and (d) SAED pattern of Cu (0.3%)-doped $Mg_2B_2O_5$ nanophosphors.

$$\frac{k}{s} = \frac{\left(1 - R_{\infty}\right)}{2R_1} = f\left(R_1\right) \quad (1)$$

where, f(R1),R_{∞},R_1,S, K is the Kubelka–Munk function, the reflectance at infinite thickness, absolute diffuse reflectance, scattering coefficient, and absorption coefficient, respectively.

Tauc's plots reveal the band gaps for various concentrations of Cu-doped magnesium pyroborate, as shown in Fig. 5. With the increase in the concentration of the dopant, the band gap decreases continuously from 5.18 eV for MBC1 to 5.10 eV for MBC3. The decrease in the band gap can be attributed to the replacement of magnesium ions by copper ions having larger ionic radii, resulting in the upward shift of the valence band decreasing the band gap of the doped samples. The lowering of the band gap also indicates the reinforcement of the strain and defect states.

Soft x-ray Absorption Near Edge Structure (XANES) Spectroscopy

Figure 6 shows the XANES spectra at the Cu L-edge and the O K-edge of pure and Cu-doped $Mg_2B_2O_5$ nanophosphors. The Li K-edge energy is very low (54.7 eV) and has a low scattering cross-section, implying that the Li K-edge XANES could not be measured due to the lower energy resolution of the beam line used at the Pohang Accelerator Laboratory.

To confirm the valence state of the Cu ions, the Cu L-edge XANES spectra were recorded for pure and 3% Cu-doped

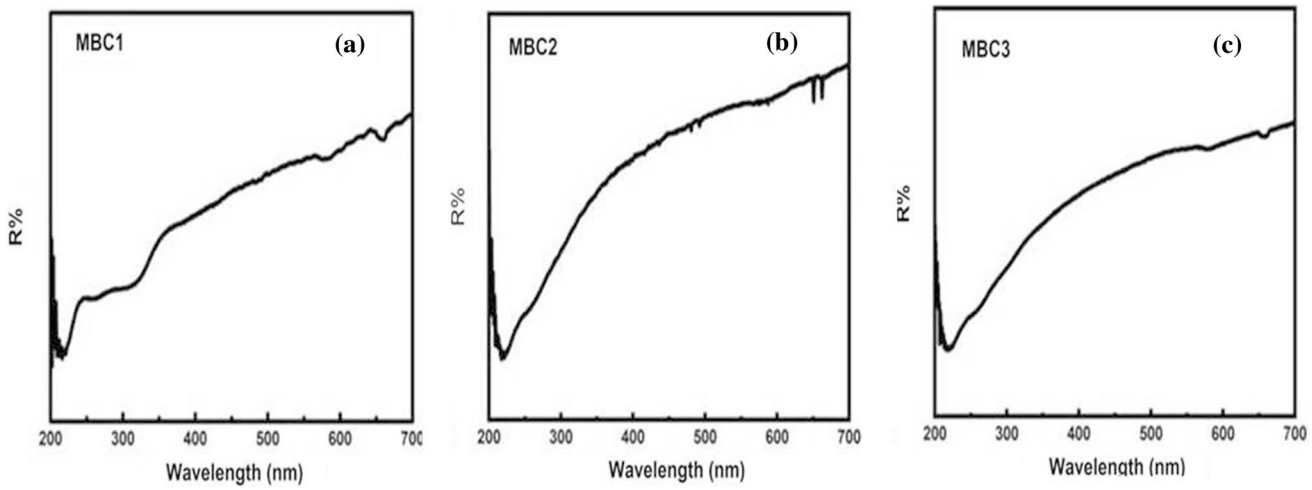

Fig. 4 Diffuse reflectance spectra of (a) Cu (0.1%)-, (b) Cu (0.2%)-, and (c) Cu (0.3%)-doped $Mg_2B_2O_5$ nanophosphors.

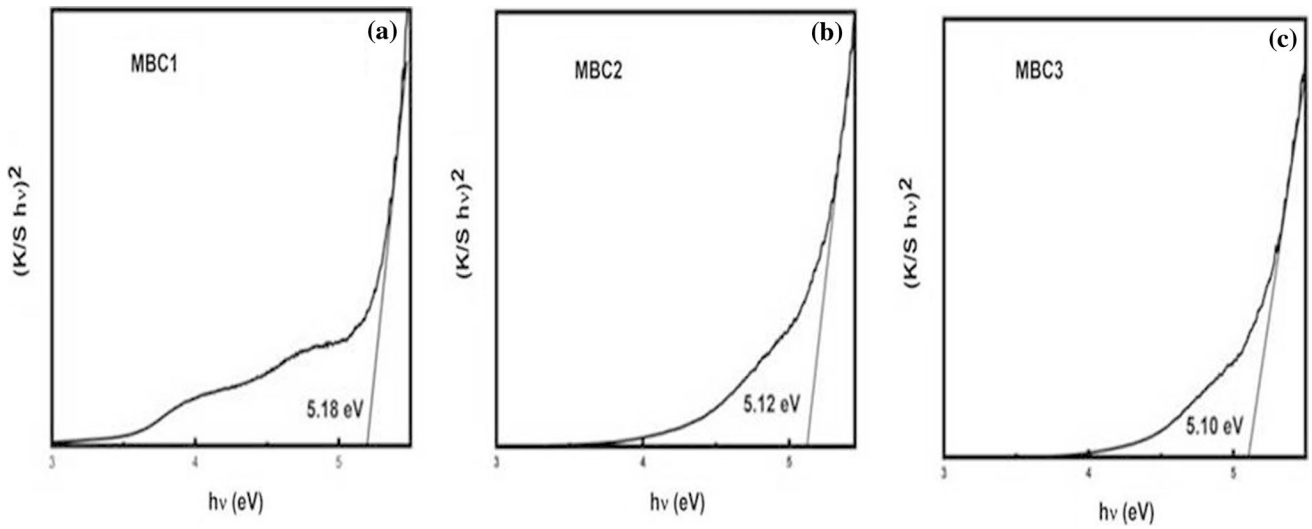

Fig. 5 Tauc's plot for (a) Cu (0.1%)-, (b) Cu (0.2%)-, and (c) Cu (0.3%)-doped $Mg_2B_2O_5$ nanophosphors.

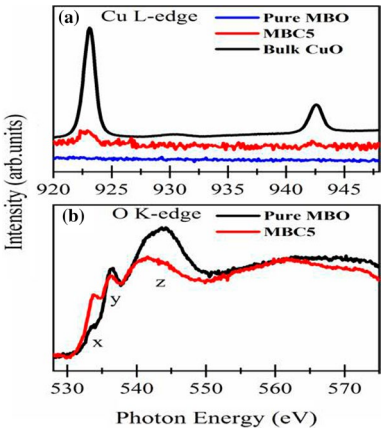

Fig. 6 (a) Cu L-edge XANES spectra from pure magnesium borate, Cu-doped (0.3%) $Mg_2B_2O_5$ nanophosphors, and bulk copper oxide. (b) O K-edge spectra from pure and Cu-doped (0.3%) $Mg_2B_2O_5$ nanophosphors.

$Mg_2B_2O_5$ nanophosphors and compared with the CuO sample as reference. From Fig. 6a, it can be seen that the Cu L-edge spectra for CuO show two distinct peaks at 922.6 eV and 942.5 eV assigned to the dipole-allowed electronic transitions from Cu $2p_{3/2}$ (L_3) and $2p_{½}$ (L_2) into the unoccupied Cu 3*d*-orbitals, respectively.[39,40] The valence state of Cu in the CuO sample is 2+ (i.e., Cu^{2+} ions).[34,35] The Cu L-edge spectrum from the pure $Mg_2B_2O_5$ does not show any peak, which demonstrates the absence of Cu ions in the sample, whereas a moderate intensity of the Cu L-edge peak is observed in the Cu-doped (3%) $Mg_2B_2O_5$. The peak position of the Cu L-edge spectrum of the Cu-doped (3%) $Mg_2B_2O_5$ samples are the same as that of the Cu L-edge spectrum from the reference CuO sample, proving the existence of Cu^{2+} ions in the Cu-doped (0.3%) $Mg_2B_2O_5$ nanophosphors. Although the intensity of Cu L-edge peaks (from Cu-doped (0.3%) $Mg_2B_2O_5$ sample) is less compared to the Cu L-edge spectrum of reference CuO sample, this is due to the low concentration of Cu^{2+} ions in the Cu-doped (3%) $Mg_2B_2O_5$ sample compared to the reference CuO sample.

Figure 6b shows the O K-edge spectra for pure and Cu (3%)-doped $Mg_2B_2O_5$ nanophosphors. The typical O K-edge spectrum of the oxide compounds arises from the dipole-allowed O 1s core electrons transition to unoccupied energy levels above the Fermi level, i.e., O 2p states hybridized with metal empty states.[41,42] Therefore, the O K-edge spectrum can map the oxygen-related *p*-projected states in the conduction band and the variation therein as a function of defects in the compounds.[36,37] The O K-edge spectrum of the pure $Mg_2B_2O_5$ sample exhibits three peaks, at 533.2 eV, 536.1 eV, and 543.9 eV. The first low intense peak (at 533.2 eV) is known as the pre-edge peak and is a dipole-forbidden peak. This peak originates from the defect states which are situated below the O 2p states.[43,44] The appearance of this peak has been reported to be related to the surface defect states or oxygen vacancies.[38,39] It can be seen from Fig. 6b that the intensity of the defect-induced peak is high, indicating the higher concentration of defect states or higher O ion vacancy formation upon doping of Cu in the $Mg_2B_2O_5$. Even though both Mg and Cu have 2+ valence states, dispersion of the Cu d states is larger than the dispersion of the Mg d bands. This may lead to a O 1s to O 2p transition at lower energy. A similar transition is clearly visible in the O K-edge spectrum of the Cu-doped $Mg_2B_2O_5$sample as the peak at 543.9 eV shifts towards a lower energy. This further suggests the insertion of Cu^{2+} ions at the substitutional sites of Mg ions in the $Mg_2B_2O_5$.

Photoluminescence Spectroscopy

To study the effect of Cu-doping on the emission properties of magnesium pyroborate nanophosphors, PL spectra at the excitation wavelength of 325 nm using a helium cadmium laser have been analyzed, as shown in Fig. 7a. The PL spectrum of 0.1% Cu-doped magnesium pyroborate comprises one broad peak with the maxima around 591 nm and another broad peak with a relatively low intensity with the maxima around 831 nm. As the concentration of the dopant is increased, the intensity of the 2nd peak starts increasing, resulting in one superposed broader single peak. The first peak with a larger intensity is due to oxygen vacancies and magnesium vacancies resulting in multiple trapping states within the band gap of the material. In this region, some emissions might be due to Cu^{2+} which emits at 528 nm, 470 nm, and 580 nm. The Cu^{2+} emission also contributes to the peak at longer wavelengths, which is due to d-d transition. Cu^{2+} forms different trapping sites resulting into emissions in the region towards the end of the spectra. Cu^{+} -assisted emissions are generally found in the range 350–400 nm, while the absence of an emission in this range indicates the absence of Cu^{+} ions in the sample. Hence, it can be concluded that the emission is due to Cu^{2+} ions. Further investigation is to be carried out in order to obtain precise information about the kinds of traps which result in emissions in this region of the electromagnetic spectrum. From the CIE diagram, it can be seen that all the samples having emissions in the yellow-reddish region of the electromagnetic spectrum.

Thermoluminescence Analysis of Copper-Doped $Mg_2B_2O_5$ Nanophosphors

TL glow curves of various concentrations of Cu-doped $Mg_2B_2O_5$nanophosphors have been recorded after exposure to gamma radiation at different doses before heat treatment, as shown in Fig. 8. The glow curve of $Mg_2B_2O_5$: Cu (0.1–0.3%) comprises one broad asymmetric peak

with a shoulder towards the high-temperature region of the curve and the maxima around 435–455 K, indicating the presence of two types of trapping sites. For the 0.1% Cu-doped sample, the TL intensity increases continuously as a function of the gamma irradiation dose in the range 50 Gy to 5 KGy, indicating the proportional increase in the charge carrier concentration with dosage facilitating the movement of electrons out from the traps. Along the same lines, the increase in TL intensity for the 0.2% and 0.3% Cu-doped samples with dosage can be attributed to the increase in the concentration of charge carriers. With the increase in dopant concentration from 0.1% to 0.2%, the maxima of the peak shifts from 455 K to 443 K, indicating the transformation of the deep trap into a shallow trap, resulting in an easier escape of electrons from the traps. On a further increment in the dopant concentration

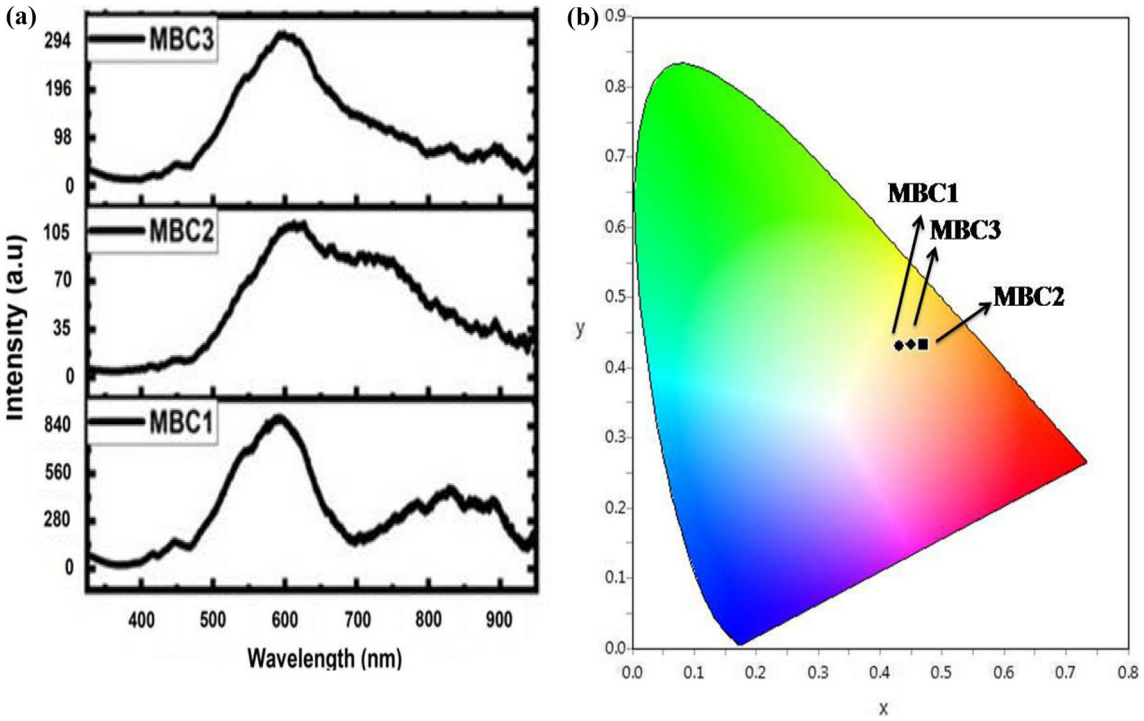

Fig. 7 (a) Photoluminescence emission spectra, (b) CIE chromaticity diagram for MBC1, MBC2, and MBC3 with x and y coordinates (0.4310, 0.4309), (0.4710, 0.4325), and (0.4499, 0.4336) respectively.

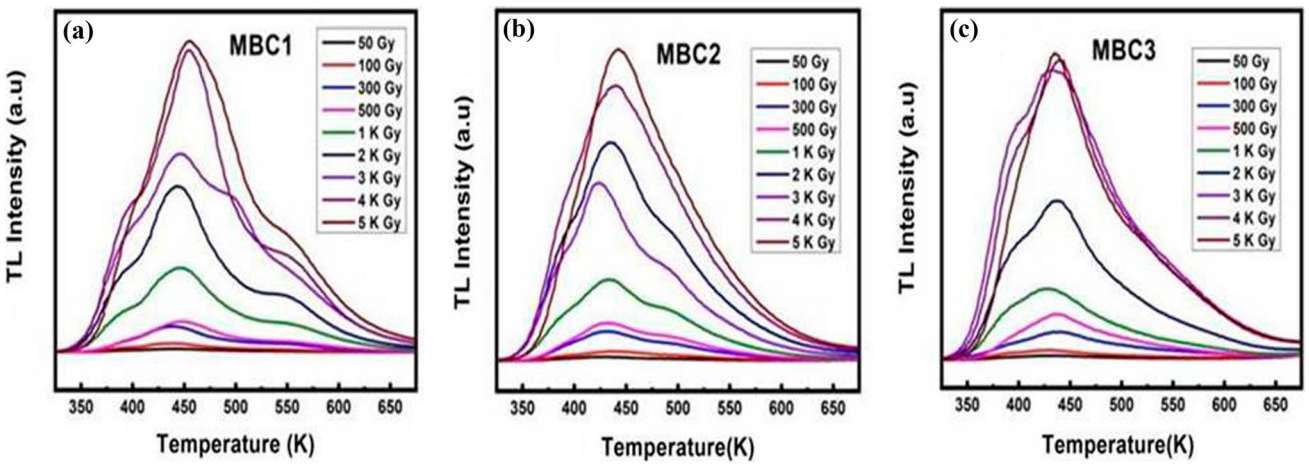

Fig. 8 Thermoluminescence glow curve for gamma-irradiated (a) Cu (0.1%)-, (b) Cu (0.2%)-, and (c) Cu (0.3%)-doped $Mg_2B_2O_5$ nanophosphors.

from 0.2% to 0.3%, the peak position shifts from 443 K to 435 K ,which points to the transformation into the shallower traps.

In order to obtain a deeper insight into the traps of the TL glow curves, deconvolution of the curves was carried out using TLanal software employing Kiti's general order equation,[45–47] in order to obtain kinetic parameters like activation energy, order of kinetics, and frequency factor. Although there are various methods, like Chen's peak shape method[48] and the initial rise method, to elucidate kinetics parameters, in this present scenario glow curves are complex. Hence, they are not implementable here. The Kiti's general order equation used in the TLanal software is:

$$I(T) = sn_0 \exp\left(\frac{E}{KT}\right)\left[1 + (b-1)\frac{s}{\beta}\exp\int\left(-\frac{E}{KT'}\right)dT'\right]^{-b(b-1)} \quad (2)$$

where I(T) is the glow peak intensity, E is the activation energy, s is the frequency factor, n_o is the initial concentration of charge carriers per cm, K is Boltzmann constant, T is the absolute temperature in kelvin, the β is the heating rate, and b is the order of the kinetics.

Figure 9 presents the deconvoluted TL glow curves for all the samples reported in the present study. It can be seen that the single broadened peak in the TL glow curve is actually generated by the superimposition of four individual peaks. The kinetic parameters obtained from deconvoluting the four underlying peaks are different, and therefore the peaks correspond to four different closely lying traps. The values of the kinetic parameters like activation energy, frequency factor, and order of kinetics are listed in Table III. From the deconvolution of the TL glow curves, it can be inferred that the distribution of traps changes with the concentration of the dopants. Also, the Cu-doped $Mg_2B_2O_5$ nanophosphor has been found to be highly sensitive to gamma radiation and therefore could be used for radiation dosimetry.

Conclusions

Single-phase triclinic $Mg_2B_2O_5$ nanophosphors doped with different concentrations of copper (0.1–0.3%) have been synthesized using a combustion technique with urea as the fuel at low temperatures. Phase formation has been confirmed using x-ray diffraction with Rietveld refinement

Table III Kinetic parameters of Cu-doped $Mg_2B_2O_5$ nanophosphors irradiated with a 5-KGy gamma dose obtained after deconvolution using TLanal software

$Mg_2B_2O_5$: Cu (0.1%)	1st Trap	2nd Trap	3rd Trap	4th Trap
Energy (eV)	0.926	0.927	1.197	0.996
s″	1.24×10^{11}	6.23×10^{9}	6.23×10^{11}	2.18×10^{8}
B	2	1.802	2	2
$Mg_2B_2O_5$:Cu (0.2%)	1st Trap	2nd Trap	3rd Trap	4th Trap
Energy (eV)	0.809	1.036	1	0.987
s″	3.19×10^{9}	1.79×10^{11}	4.28×10^{9}	1.82×10^{8}
B	1.54	2	2	2
$Mg_2B_2O_5$:Cu (0.3%)	1st Trap	2nd Trap	3rd Trap	4th Trap
Energy (eV)	1.018	1	0.197	1.010
s″	2.61×10^{12}	9.77×10^{10}	6.34×10^{8}	3.15×10^{8}
B	2	2	2	2

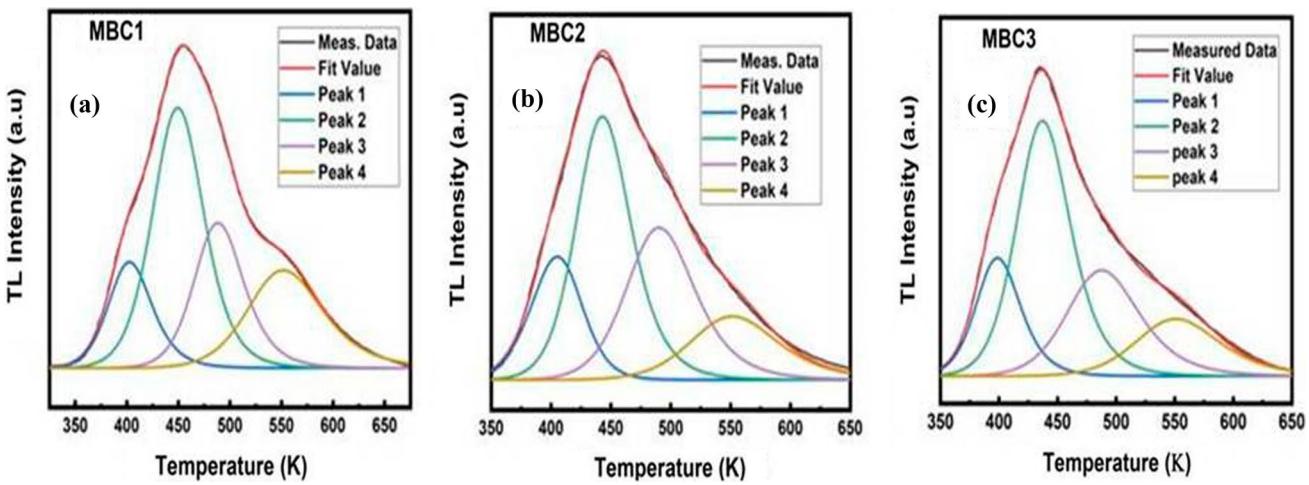

Fig. 9 Deconvoluted TL glow curves irradiated with 5-KGy gamma radiations for (a) Cu (0.1%)-, (b) Cu (0.2%)-, and Cu (0.3%)-doped $Mg_2B_2O_5$ nanophosphors.

of the diffraction patterns, TEM, HR-TEM and SAED. Band gaps of the samples have been calculated from the Kubelka–Munk function for $Mg_2B_2O_5$: Cu (0.1–0.3%) in the range 5.10–5.18 eV. XANES study predicted the presence of oxygen vacancies and the substitution of Mg^{2+} ions by Cu^{2+} ion. PL properties show emissions in the yellow-reddish visible region due to Cu^2, oxygen, and magnesium vacancies. TL analysis of gamma-irradiated nanophosphors show the presence of four closely lying traps having different kinetics parameters, while the distributions of these traps changes with the concentration and gamma radiation dose. This study has shown that Cu-doped magnesium pyroborate could be used for various applications like radiation dosimetry and other luminescence-based applications.

Acknowledgments The authors are grateful to DST New Delhi for DST-FIST project in Physical Sciences with Grant No. SR/FST/PS-I/2019/68. We also thank Director IUAC-New Delhi for granting permission to conduct HR-TEM and TL experiments. Thanks are due to Mr. Ambuj Mishra and Mr. Birender Kumar for their support in HR-TEM and TL measurements.

Conflict of interest The authors declare that they have no known competing financial interests or personal relationships that could have appeared to influence the work reported in this paper.

References

1. C. Helvaci, MINERALS|Borates, Editor(s): Richard C. Selley, L. Robin M. Cocks, Ian R. Plimer, Encyclopedia of Geology, Elsevier, Pages 510-522, ISBN 9780123693969, https://doi.org/10.1016/B0-12-369396-9/00279-3 (2005). (http://www.sciencedirect.com/science/article/pii/B0123693969002793)
2. E. Pekpak, A. Yılmaz, and G. Özbayoglu, An overview on preparation and TL characterization of lithium borates for dosimetric use. *Int .J. Miner Process.* 3, 14–24 (2010).
3. J. Cao, J. Cao, S. Pan, H. Yu, W. Zhao, and Z. Yang, Synthesis, crystal structure and properties of a new strontium cadmium diborate. *Inorganica Chim. Acta.* 392, 459–464 (2012).
4. T. Kitamura, K. Sakane, and H. Wada, Formation of needle crystals of magnesium pyroborate. *J. Mater. Sci. Lett.* 7, 467 (1988).
5. W. Li, Z. Jin, and Z. Zhang, Application and synthesis of inorganic whisker materials. *Prog. Chem.* 15, 264 (2003).
6. S. Bian, J. Li, X. Nai, and W. Li, Preparation of $Mg_2B_2O_5$ whisker and preliminary study on its growth mechanism. *J. Salt Lake Res.* 15, 45 (2007).
7. X. Tao, and X. Li, Catalyst-free synthesis, structural and mechanical characterization of twinned $Mg_2B_2O_5$ nanowires. *Nano Lett.* 8, 505 (2008).
8. Y. Li, Z. Fan, J.G. Lu, and R.P.H. Chang, Synthesis of magnesium borate ($Mg_2B_2O_5$) nanowires by chemical vapor deposition method. *Chem. Mater.* 16, 2512 (2004).
9. Y. Zheng, H. Yang, W. Fu, L. Qiao, L. Chang, and J. Chen, Synthesis of magnesium Borate (Mg2B2O5) nanowires, growth mechanism and their lubricating properties. *Mater. Res. Bull.* 43, 2239 (2008).
10. E.M. Elssfah, A. Elsanousi, J. Zhang, H.S. Song, and C. Tang, Synthesis of magnesium borate nanorods. *Mater. Lett.* 61, 4358–4361 (2007).
11. L. Yan, F. Zhiyong, G.L. Jia, and R.P.H. Chang, Synthesis of magnesium borate ($Mg_2B_2O_5$) nanowires by chemical vapor deposition method. *Chem. Mater.* 16, 2512–2514 (2004).
12. X. Tao, and X. Li, Catalyst-free synthesis, structural, and mechanical characterization of twinned $Mg_2B_2O_5$ nanowires. *Nano Lett.* 8, 505–510 (2008).
13. W. Zhu, X. Zhang, L. Xiang, and S. Zhu, Hydrothermal formation of the head-to-head coalesced szaibelyite $MgBO_{(2)}(OH)$ nanowires. *Nanoscale Res. Lett.* 4, 724–731 (2009).
14. R.Z. Ma, Y. Bando, and T. Sato, Nanowires of metal borates. *Appl. Phys. Lett.* 81, 3467–3469 (2002).
15. R.Z. Ma, Y. Bando, D. Golberg, and T. Sato, Nanotubes of magnesium borate. *Chem. Int. Ed.* 42, 1836–1838 (2003).
16. T.M. Oliveira, A.F. Lima, M.G. Brik, S.O. Souza, and M.V. Lalic, Electronic structure and optical properties of magnesium tetraborate: An ab initio study. *Comput. Mater. Sci.* 124, 1–7 (2016).
17. S. İflazoğlu, A. Yılmaz, V.E. Kafadar, M. Topaksu, and A.N. Yazıcı, Neutron Gamma response of undoped and Dy doped MgB_4O_7 thermoluminescence dosimeter. *Appl Radiat Isot.* 147, 91–98 (2019).
18. L. Wang, L. Cong, Y.S. Zhang, Y.Q. Wang, D.M. Cao, X.P. Huang, and Y. Liu, Synthesis of magnesium borate ($Mg_2B_2O_5$) whisker by flux method. *Adv Mat Res.* 287–290, 683–687 (2011).
19. L. Wang, Y. Zhang, D. Chen, Y. Liu, Y. Wang, Z. Dong, Y. Lu, and X. Huang, A cost-effective process for synthesizing magnesium borate nanorods and its mechanical property for reinforced nylon-6 composites. *NANO* 9, 1450078 (2014).
20. W. Wang, J. Wang, A. Deng, L. Wang, H. Shi, and Y. Liang, Synthesis and growth mechanism of whisker-like $Mg_2B_2O_5$ crystals by an easy and environmentally hospitable non-aqueous ionic liquid method. *Micro Nano Lett.* 10, 130–134 (2015).
21. W. Zhu, Q. Zhang, L. Xiang, F. Wei, X. Sun, X. Piao, and S. Zhu, Flux-assisted thermal conversion route to pore-free high crystallinity magnesium borate nanowhiskers at a relatively low temperature. *Cryst. Growth Des.* 8, 2938–2945 (2008).
22. W. Zhu, G. Li, Q. Zhang, L. Xiang, and S. Zhu, Hydrothermal mass production of $MgBO_2(OH)$ nanowhiskers and subsequent thermal conversion to $Mg_2B_2O_5$nanorods for biaxially oriented polypropylene resins reinforcement. *Powder Technol.* 203, 265–271 (2010).
23. O. Sheng, C. Jin, J. Luo, H. Yuan, H. Huang, Y. Gan, J. Zhang, Y. Xia, C. Liang, W. Zhang, and X. Tao, $Mg_2B_2O_5$ nanowire enabled multifunctional solid-state electrolytes with high ionic conductivity excellent mechanical properties, and flame-retardant performance. *Nano Lett.* 18, 3104–3112 (2018).
24. G. Dou, M. Guo, Y. Li, and J. Lin, The effect of LMBS glass on the microwave dielectric properties of the $Mg_3B_2O_6$ for LTCC. *J. Mater. Sci.: Mater. Electron.* 26, 4207–4211 (2015).
25. Y. Zeng, H. Yang, W. Fu, L. Qiao, L. Chang, J. Chen, H. Zhu, M. Li, and G. Zou, Synthesis of magnesium borate ($Mg_2B_2O_5$) nanowires, growth mechanism and their lubricating properties. *Mater. Res. Bull.* 43, 2239–2247 (2008).
26. A.F. Qasrawi, T.S. Kayed, A. Mergen, and M. Gürü, Synthesis and characterization of $Mg_2B_2O_5$. *Mater. Res. Bull.* 40, 583–589 (2005).
27. A.B. Awatif and E.M. Elssfah, From monoclinic $Mg_2B_2O_5$ nanowires to triclinic $Mg_2B_2O_5$: Eu nanorods. *Elixir Nanotechnol.* 75, 27521–27524 (2014).
28. J. Kumar, A. Sharma, S.O. Won, R. Kumar, K.H. Chae, S. Kumar, and A. Vij, Probing defects and electronic structure of Eu-doped t-$Mg_2B_2O_5$ nanocrystals using X-ray absorption near

edge spectroscopy and luminescence techniques. *Vacuum* 180, 109602 (2020). https://doi.org/10.1016/j.vacuum.2020.109602.
29. J. Kumar, S. Kumar, C. Shekhar, R. Brajpuriya, and A. Vij, Effect of Eu-doping on the thermoulminescence of UV and gamma irradiated $Mg_2B_2O_5$ nanophosphors. *Luminescence* (2021). https://doi.org/10.1002/bio.4197.
30. J. Kumar, R. Kumar, M. Singh, S. Kumar, R. Kumar, S.O. Won, R. Brajpuriya, S. Dwivedi, R.K. Sharma, and A. Vij, Structural, diffuse reflectance and luminescence study of t-$Mg_2B_2O_5$ nanostructures. *Appl. Phys. A* 127, 617 (2021).
31. J.C. Fernandes, F.S. Sarrat, R.B. Guimaraes, R.S. Freitas, M.A. Continentino, A.C. Doriguetto, Y.P. Mascarenhas, J. Ellena, E.E. Castellano, J.-L. Tholence, J. Dumas, and L. Ghivelder, Structure and magnetism of $MnMgB_2O_5$ and $Mn_2B_2O_5$. *Phys. Rev. B* 67, 104413 (2003).
32. F. J. Glass Hugh, L. Zigeng, M. Bayley Paul, S. Emmanuelle, B. Shou-Hang, G. Khalifah Peter, P. Grey Clare, and E. Dutton Siân, *Chemistry of Materials*, 29(7), 3118–3125 (2017).
33. P.O. Ike, D.E. Folley, C.D. Umeh, K.K. Agwu, M.L. Chithambo, S. Chikwembani, and F.I. Ezema, The effect of copper on the structural and thermoluminescence properties of aluminium borate. *J. Lumin.* 226, 117504 (2020).
34. R.R. Patil, S.V. Moharil, S.M. Dhopte, P.L. Muthal, and V.K. Kondawar, Thermoluminescence in some Cu-doped compounds. *Phys. Stat. Sol.* 199, 527–532 (2003).
35. J. Kumar, A. Yadav, P.A. Alvi, S. Kumar, A. Vij, Combustion synthesis and thermoluminescence response of near UV irradiated $Mg_2B_2O_5$ nanophosphors. *AIP Proceedings* (2019) 2093.
36. Sharma, J.P. Singh, S.O. Won, K.H. Chae, S.K. Sharma, S. Kumar, Introduction to X-Ray Absorption Spectroscopy and its applications in material science, Ed. by S. Sharma (Handbook of Materials Characterization, Springer (2018) 497–548
37. G.-C. Guo, W.-D. Cheng, J.-T. Chen, J.-S. Huang, and Q.-E. Zhang, Triclinic $Mg_2B_2O_5$. *Acta Cryst. C* 51, 351 (1995).
38. J.L.C. Rowsell, N.J. Taylor, and L.F. Nazar, Crystallographic investigation of the Co–B–O system. *J. Solid State Chem.* 174, 189 (2003).
39. M. Sharma, J. Varshney, T.K. Park, K.H. Ha, and H.J. Chae, Shin, XANES, EXAFS and photocatalytic investigations on copper oxide nanoparticles and nanocomposites. *RSC Adv.* 5, 21762 (2015).
40. M. Sharma, H.J. Varshney, B.H. Shin, K.H. Lee, and S.O. Chae, Won, Effect of Cu insertion on structural, local electronic/atomic structure and photocatalyst properties of TiO_2, ZnO and $Ni(OH)_2$ nanostructures: XANES-EXAFS study. *Mater. Chem. Phys.* 191, 129–144 (2017).
41. M. Sharma, K.H. Varshney, H.J. Chae, and S.O. Shin, Won, Investigation on the local electronic/atomic structure properties using XANES/EXAFS and photocatalyst application of $Zr_{1-x}Cu_xO_2$ ($0 \leq x \leq 0.2$). *Curr. Appl. Phys.* 16, 1326–1333 (2016).
42. M. Sharma, W.C. Varshney, H.J. Lim, J.P. Shin, S.O.W. Singh, and K.H. Chae, Mechanistic insights on the electronic properties and electronic/atomic structure aspects in orthorhombic $SrVO_3$ thin films: XANES–EXAFS study. *Phys. Chem. Chem. Phys.* 19, 6397–6405 (2017).
43. S. Chaudhary, H. Saraswat, D. Devi, P. Kulriya, F. Singh, S.O. Won, H.J. Shin, J. Parkash, and A. Sharma, Structural and electronic-structure investigations of defects in Cu-ion-implanted SnO_2 thin films. *Vacuum* 179, 109481 (2020).
44. H. Saraswat, S. Chaudhary, M. Varshney, D. Devi, F. Singh, S.O. Won, H.J. Shin, and A. Sharma, *Vacuum* 181, 109655 (2020).
45. C. Furetta, G. Kitis, P.S. Weng, and T.C. Chu, Thermoluminescence characteristics of MgB4O7: Dy, Na. *Nucl. Instrum. Methods Phys. Res. A.* 420, 441–445 (1999).
46. G. Kitis, and V. Pagonis, Peak shape methods for general order thermoluminescence glow-peaks: A reappraisal. *Nucl. Instrum. Methods Phys. Res. B.* 262, 313–322 (2007).
47. S. Kumar, A.K. Gathania, A. Vij, and R. Kumar, Gamma induced thermoluminescence and color centers study of Dy doped LiF micro-cubes. *Ceram. Int.* 42, 14511–14517 (2016).
48. S. Kumar, A.K. Gathania, A. Vij, A.K. Sharma, R. Dogra, S.P. Lochab, and R. Kumar, Absorption, photoluminescence and thermoluminescence studies of γ- irradiated pure and Eu-doped LiF phosphors. *Adv. Mater. Lett.* 6, 620–627 (2015).